

Transfer impedance calculations of electronic noise in two-terminal semiconductor structures

E. Starikov, P. Shiktorov, and V. Gružinskis
Semiconductor Physics Institute, A. Goštauto 11, 2600 Vilnius, Lithuania

L. Varani, J. C. Vaissiere, and J. P. Nougier
Centre d'Electronique et de Micro-optoélectronique de Montpellier, (CNRS UMR 5507) Université Montpellier II, 34095 Montpellier Cedex 5, France

T. González, J. Mateos, and D. Pardo
Departamento de Física Aplicada, Universidad de Salamanca, Plaza de la Merced s/n, 37008 Salamanca, Spain

L. Reggiani
Istituto Nazionale di Fisica della Materia, Dipartimento di Scienza dei Materiali, Università di Lecce, Via Arnesano, 73100 Lecce, Italy

(Received 31 July 1997; accepted for publication 20 October 1997)

The time-domain formulation of the transfer-impedance method is developed to calculate the impedance field of two-terminal semiconductor structures. The voltage noise spectrum associated with velocity fluctuations is then calculated for overmicron and submicron n^+nn^+ GaAs diodes in the framework of a closed hydrodynamic approach based on the velocity and energy conservation equations. Transit-time effects are found to influence substantially the noise spectrum in a wide frequency range above 10 GHz. The good agreement found with Monte Carlo simulations validates the proposed theoretical approach. © 1998 American Institute of Physics.
[S0021-8979(98)04403-X]

I. INTRODUCTION

Advances in communication and information processing increasingly depend on the improvement of sensitivity and operation speed of microwave devices based on various semiconductor homostructures and heterostructures. For this sake, as guide lines of modern solid-state electronics, the following trends are emerged in recent years:¹ (i) downsizing towards the submicron and nanometric scale length, (ii) layered structures with complicated geometry and doping profile, (iii) ballistic and quantum transport, (iv) new materials and effects, etc. The common perspective of the above trends is to increase the operation frequency up to the terahertz region when sufficiently high electric fields are applied. In particular, near- and submicron n^+nn^+ GaAs, InP and Si structures form the basis for various high-frequency semiconductor devices such as transferred electron oscillators, field-effect transistors, switchers, etc. Due to their small size, extremely high electric fields (over 100 kV/cm) are locally present even for low applied voltages. As a consequence, several dynamical effects such as quasi-ballistic transport, velocity overshoot, nonlocal heating of carriers, etc. play an essential role in determining their electrical characteristics. An inherent difficulty faced by the above trends is that high fields are responsible for excess hot-carrier noise not yet thoroughly studied in submicron structures at microwave frequencies. Moreover, due to the complex geometry of these devices and the large variety of physical effects involved on such short space/time scales, a microscopic analysis of their performances becomes a rather complicated task. As a consequence, the advantages which high technology

promises in producing advanced structures do not necessarily lead to an adequate improvement of the transport and noise performances which are of importance for small-signal data processing. Due to these reasons, a theoretical analysis aiming at predicting the noise characteristics of the device performances is a mandatory issue in the research and development of advanced semiconductor structures.²

At present, two basic approaches are used to calculate hot-carrier noise in small semiconductor devices depending on the nature of the simulation procedure, respectively denoted as stochastic and deterministic.

The stochastic approach concerns with the simulation of carrier transport by a stochastic procedure such as the Monte Carlo Particle (MCP) method,³⁻⁷ which already includes the microscopic fluctuations of the velocity and energy of single particles. In the framework of this approach widely used in the last years⁸⁻⁴⁰ a multiparticle history is simulated during a sufficiently long time interval, the correlation functions of current or voltage fluctuations are then calculated in a natural way by using the time averaging over the simulated history and the appropriate spectral densities are finally calculated from the Wiener-Khitchine theorem. The advantage of the MCP approach is based on the direct incorporation of any details of the band structure, scattering mechanisms, device design, etc. into the simulation which gives the exact solution of the appropriate kinetic equation self-consistently coupled with a Poisson solver. However, the physical information about the processes responsible for the device performance and electronic noise is obtained from the analysis of the time and frequency behavior of the correlation functions

of various fluctuating quantities and their spectral densities. Since this information is given already in an integrated form, it is often difficult to separate various processes, to determine their importance, and to perform the decomposition of the total noise in terms of the local sources and small-signal coefficients.

In the framework of a deterministic procedure which does not include in itself microscopic fluctuations, the field-impedance method and its generalization^{41–43} has been recognized as a powerful method for noise calculations. This method connects the local fluctuations of the single-particle velocities inside the device with the fluctuations of the voltage drop between two probing terminals. For the simple but significant case of a one dimensional geometry in real space, the impedance field method provides the expression

$$S_U(\omega) = Ae^2 \int_0^L n(x) |\nabla Z(x, \omega)|^2 S_v(x, \omega) dx, \quad (1)$$

where $S_U(\omega)$ is the spectral density of the voltage fluctuations between the terminals as measured under constant current operation, $\omega = 2\pi f$ the circular frequency, e the electric charge, A the cross-sectional area of the device, L the length of the device between the probing electrodes taken along the x direction, $n(x)$ the local carrier concentration, $\nabla Z(x, \omega)$ the impedance field, and $S_v(x, \omega)$ the local spectral density of velocity fluctuations. The impedance field relates the perturbation of the total voltage drop U between the terminals with the perturbation of the conduction current-density j_d at a point x_0 through

$$\delta U(x_0; \omega) = \nabla Z(x_0; \omega) \delta j_d(x_0; \omega). \quad (2)$$

In Eq. (2), which pertains to the frequency domain, we retain the variable x_0 in δU to emphasize that the origin of the perturbation is in x_0 . We stress that Eq. (1) strictly separates the origin of the fluctuations, represented by the local source, from their spatio-temporal evolution, represented by the impedance field. Moreover, the spectral density of voltage fluctuations of the whole device is represented as a sum of contributions belonging to different parts of the structure. Therefore, on the one hand, this approach can be considered as the most powerful tool for detailed investigations of the noise spatial distribution throughout the device. On the other hand, in a seminal paper van Vliet *et al.*⁴² proved that the impedance field can be derived from a more general two-point function called transfer impedance relating the source of the perturbation with any point in the structure. In turn, the transfer impedance can be connected with the Green function of the linearized voltage response. This gives the additional possibility to investigate directly the spatio-temporal evolution of single electrical perturbations (fluctuations) induced in any point of the structure, which is a very difficult task in stochastic procedures.

For velocity fluctuations, the local noise source is given by the field dependence of the longitudinal diffusion coefficient used in the framework of a local field approximation, and $n(x)$ and $\nabla Z(x, \omega)$ are obtained using a drift-diffusion (DD) approach for the conduction current.^{42,44–48} However, these approximations are known to fail in submicron space scales due to nonlocal heating of carriers when the carrier

energy no longer corresponds directly to the local electric field, especially for semiconductors exhibiting a substantial overshoot effect of the drift velocity e.g., GaAs.^{49–53}

The aim of this work is to apply the impedance field method and its transfer extension to the hydrodynamic (HD) transport model based on the velocity and energy conservation equations. The HD approach is in fact more realistic for the case of submicron devices,^{37,54,55} since it allows to account for the velocity overshoot, the nonlocality of hot-carrier heating and other effects inherent to the small-space scale. Thus, the main attention will be paid to submicron structures even if, to better understand the analogies and the main differences between the features of small- and large-space scales, some results for a long diode (of about 10 μm length) will be reported for comparison.

The article is organized as follows. In Sec. II we describe the closed HD model and present a procedure for the numerical calculation of the impedance-field spectrum $\nabla Z(x_0; \omega)$ and related quantities making use of the transfer-impedance method. Section III presents the relevance of the procedure which is illustrated by calculating the small-signal and various noise characteristics in submicron n^+nn^+ GaAs diodes. The main conclusions are summarized in Sec. IV.

II. THEORY

Usually two main modes of operation are of importance in two-terminal devices. In the former a constant voltage is applied between the structure terminals and the fluctuating macroscopic quantity is the conduction current flowing through the device. In the latter, a constant total current is forced to flow through the structure and the fluctuating macroscopic quantity is the voltage drop between the terminals of the device. In both modes the microscopic origin of the fluctuations is the velocity of single particles inside the structure which, in turn, leads to local fluctuations of the carrier concentration, the conduction current, and the self-consistent electric field. Since in the former operation mode the integral of the electric field throughout the structure, that is the applied voltage, is constant, a local fluctuation of the electric field leads to a redistribution of the electric field inside the whole sample. Thus, a single fluctuation of the electric field under constant voltage operation becomes immediately coupled with fluctuations in all other points of the device and, strictly speaking, the noise becomes non-local. This complicates considerably the interpretation of single fluctuations and their decomposition into separate contributions to the total noise. For the constant-current operation mode, such an integrated coupling is absent. This offers the possibility to consider the spatio-temporal evolution of single fluctuations inside the structure, and to relate the local microscopic fluctuations with the macroscopic voltage fluctuations by using the transfer-impedance and impedance-field approaches. For this purpose, the main system of equations is usually formulated in such a way that the fundamental electrical variable to be represented is the local electric field.

A. The model

To simulate constant-current operation mode, we use the definition of the total current-density, J , taken to be constant in time and, for the one-dimensional geometry here considered, also constant in space:

$$J = en(x,t)v(x,t) + \epsilon\epsilon_0 \frac{\partial E(x,t)}{\partial t} = \text{const}, \quad (3)$$

where $v(x,t)$ is the carrier local average velocity, ϵ_0 the vacuum permittivity, ϵ the relative static dielectric constant of the material, and $E(x,t)$ the instantaneous local electric field. Then the Poisson equation writes

$$n(x,t) = N_d(x) + \frac{\epsilon\epsilon_0}{e} \frac{\partial E(x,t)}{\partial x}, \quad (4)$$

$N_d(x)$ being the donor concentration profile. After the substitution of Eq. (4) in Eq. (3) we obtain an equation for the electric field $E(x,t)$ in the form

$$\frac{\partial E}{\partial t} + v \frac{\partial E}{\partial x} + \frac{e}{\epsilon\epsilon_0} v N_d = \frac{1}{\epsilon\epsilon_0} J. \quad (5)$$

To close the system of Eqs. (4) and (5) it is necessary to define the average velocity of carriers. It must be stressed that in the general case this definition can be made by using rather different approaches such as the DD, the extended drift diffusion (EDD), various HD, or even some simplified models. For example, by assuming that v is a function of the local electric field only, one recovers the approach firstly used by van Vliet *et al.* in Ref. 42; the implementation of the DD approach gives the time-domain formulation of the impedance-field method developed by Ghione *et al.*,^{46–48} etc. Here we shall describe the carrier transport in the framework of the conservation equations for the carrier average-velocity $v(x,t)$ and mean-energy $\epsilon(x,t)$ written in the form^{55,56}

$$\frac{\partial v}{\partial t} = eEm^{-1} - v\nu_v - v \frac{\partial v}{\partial x} - \frac{1}{n} \frac{\partial}{\partial x} (nQ_v), \quad (6)$$

$$\frac{\partial \epsilon}{\partial t} = eEv - (\epsilon - \epsilon_{th})\nu_\epsilon - v \frac{\partial \epsilon}{\partial x} - \frac{1}{n} \frac{\partial}{\partial x} (nQ_\epsilon). \quad (7)$$

Equations (6) and (7) contain five energy parametric dependencies, namely, the average of the reciprocal effective mass m^{-1} in the direction of the electric field E , the velocity and energy relaxation rates, ν_v and ν_ϵ , the variance of velocity-velocity fluctuations, $Q_v = \langle \delta v^2 \rangle_0$, and the covariance of velocity-energy fluctuations, $Q_\epsilon = \langle \delta v \delta \epsilon \rangle_0$, where brackets mean average over the hot-carrier distribution function in the momentum space, and the subscript 0 indicates steady-state conditions under constant and homogeneous applied electric field. All the parameters are assumed to depend only on the local mean energy, and as such they can be obtained from a stationary MCP simulation of the bulk semiconductor.

Equations (4) and (5) together with the velocity and energy conservation Eqs. (6) and (7) constitute a closed system which allows one both: to calculate the steady-state characteristics and to investigate the spatio-temporal evolution of various perturbations responsible for the small-signal response and the electronic noise in the structure. First of all,

the stationary profiles of the electric field, concentration, velocity, and energy are calculated for a given value of the total current J . To this purpose, at the initial time moment $t=0$ reasonable starting values for $E(x,0)$, $n(x,0)$, $v(x,0)$, and $\epsilon(x,0)$ are chosen (for example, those obtained by a previous modeling of the same structure with lower values of J , or the initial conditions $n=N_d(x)$, $E(x)=0$, etc. for $J=0$ at the first modeling of the structure). Then a direct numerical solution of Eqs. (4)–(7) implements a self-consistent procedure for modeling the time evolution of $E(x,t)$, $n(x,t)$, $v(x,t)$, and $\epsilon(x,t)$ under constant total current flowing through the structure both in time and space. Since under constant current operation mode a stationary stable state of the system always exists, after all the relaxation processes are finished the stationary profiles $E_s(x)$, $n_s(x)$, $v_s(x)$, and $\epsilon_s(x)$ are achieved. The obtained steady-state profiles are then used for further calculations of the appropriate Green and response functions as described below.

B. Response-function modeling and small-signal impedance calculations

To obtain the local differential impedance and the small-signal impedance of the whole structure, the response of the device to a global perturbation of the total current J is of importance.⁵⁴ At a given initial time $t=0$ a spatially homogeneous time-impulsive delta-like perturbation of the total current [i.e., of the r.h.s. of Eq. (5)], $\delta J = \delta J_0 \delta(t)$, is introduced. By supposing that the conduction current $j_d = env$ is not perturbed at $t=0$, the time integration of Eq. (3) leads to an homogeneous perturbation of the local electric field in each point of the structure in the form

$$\delta E(x,0) = \delta E_0 = \delta J_0 / \epsilon\epsilon_0. \quad (8)$$

From a physical point of view such a perturbation corresponds to the perturbation of only the displacement component of the total current. It means that a step-like change of the voltage drop between the terminals of the structure, $\delta U_0 = L \delta E_0$ (L being the total length of the device) instantaneously appears at $t=0$ and results only in a homogeneous perturbation of the electric field which is accompanied by no variations of carrier concentration, velocity and energy. Then, a numerical solution of Eqs. (4)–(7) with the initial conditions given by Eq. (8) gives the spatio-temporal response of the device to such a perturbation. The response function of the local electric field in each point of the device is then defined as

$$D_E(x,t) = \frac{\delta E(x,t)}{\delta J_0} = \frac{1}{\epsilon\epsilon_0} \frac{E(x,t) - E_s(x)}{\delta E_0}, \quad (9)$$

where $E(x,t)$ and $E_s(x)$ are the solutions of the perturbed and unperturbed system of Eqs. (4)–(7). By Fourier transforming Eq. (9), one obtains the differential impedance, $\nabla Z'(x,\omega)$ as

$$\nabla Z'(x,\omega) = \int_0^\infty D_E(x,t) \exp(-i\omega t) dt, \quad (10)$$

which relates the linear response of the electric field $\delta E_\omega(x)$ to a small harmonic perturbation of the total current $\delta J_\omega(x)$ at frequency ω and point x as

$$\delta E_\omega(x) = \nabla Z'(x, \omega) \delta J_\omega(x). \quad (11)$$

For the one-dimensional structure considered here, the total current is constant in space, and the spatial integration of Eq. (11) throughout all the structure gives

$$\delta U_\omega = Z(\omega) \delta J_\omega. \quad (12)$$

Here δU_ω is the linear response of the terminal voltage drop caused by a harmonic perturbation of the total current and $Z(\omega)$ the small-signal impedance of the whole device defined as

$$Z(\omega) = \int_0^L \nabla Z'(x, \omega) dx. \quad (13)$$

Thus the small-signal response of the device is determined by the local response of the electric field to a global perturbation of the total current.

C. Green-function and transfer-impedance modeling

Let us consider now the local response of the structure to a local perturbation of the current which forms the basis for noise calculations. Since J is taken to be constant both in time and space, only the fluctuations of the conduction current-density $j_d = env$ are responsible for the noise. From a physical point of view the noise source can be connected with fluctuations of the electron concentration due to generation-recombination processes, with fluctuations of the carrier velocity because of the scattering processes, etc. By neglecting the physical nature of these fluctuations, let us assume that a perturbation of the conduction component of the total current given by

$$\delta j_d = \Delta \delta(x - x_0) \delta(t). \quad (14)$$

Δ being an appropriate amplitude, appears at point $x = x_0$ and initial time $t = 0$. As follows from Eqs. (4) and (5), this perturbation leads to instantaneous variations of the local electric field and carrier concentration in the form

$$\delta E(x) = -\Delta \frac{1}{\epsilon \epsilon_0} \delta(x - x_0), \quad (15)$$

$$\delta n(x) = -\Delta \frac{1}{e} \frac{\partial}{\partial x} \delta(x - x_0), \quad (16)$$

where, in practical calculations, the spatial dependence of the initial perturbation is taken of Gaussian form:

$$\delta(x - x_0) \approx \frac{1}{\gamma \pi^{1/2}} \exp\left[-\frac{(x - x_0)^2}{\gamma^2}\right]. \quad (17)$$

In numerical calculations the value of γ is taken equal to a few meshes of x space. By assuming that the initial perturbations are small enough to satisfy linearization, the difference between the time-dependent perturbed solution, $E(x, x_0, t)$, and the steady-state solution of the unperturbed system, $E_s(x)$, gives the Green function:

$$G(x, x_0, t) = \frac{\delta E(x, x_0, t)}{\Delta} = \frac{E(x, x_0, t) - E_s(x)}{\Delta}, \quad t \geq 0, \quad (18)$$

which describes the spatio-temporal evolution of the electric field perturbation caused by the local perturbation of the conduction current at point x_0 . It should be stressed that the Green function defined by Eq. (18) describes the spatio-temporal evolution of a single perturbation (or fluctuation) appearing at point x_0 of the structure. Thus, by considering the evolution of perturbations placed in various points of the structure, one can obtain additional information about the influence of several physical processes in the structure to the voltage noise in the whole device.

The Fourier transformation of the Green function gives the transfer impedance

$$z(x, x_0, \omega) = \int_0^\infty G(x, x_0, t) \exp(-i\omega t) dt, \quad (19)$$

which relates the linear response of the electric field in point x to a small harmonic perturbation of the conduction current $\delta j_{d\omega}(x_0)$ of frequency ω at point x_0 .^{42,43}

D. The impedance field

In the time-domain representation, the response of the voltage drop between the terminals of the device placed at points 0 and L caused by a conduction current perturbation at point x_0 is given by

$$\delta U(x_0, t) = \int_0^L \delta E(x, x_0, t) dx. \quad (20)$$

It is worthwhile to characterize this response by the corresponding response function which, in full analogy with Eq. (9), can be written as

$$R(x_0, t) = \frac{\delta U(x_0, t)}{\Delta} = -\frac{1}{\epsilon \epsilon_0} \frac{\delta U(x_0, t)}{\delta U(x_0, 0)}. \quad (21)$$

By Fourier transforming Eq. (21), one obtains the impedance field, $\nabla Z(x_0, \omega)$ as

$$\nabla Z(x_0, \omega) = \int_0^\infty R(x_0, t) \exp(-i\omega t) dt, \quad (22)$$

which, in accordance with Eq. (2), relates the linear response of the voltage drop between points 0 and L , $\delta U_\omega(x_0)$, to a small harmonic perturbation of the conduction current $\delta j_{d\omega}(x_0)$.

E. Spectral density of voltage and current fluctuations

By using the impedance field, the local contribution of point x to the spectral density of voltage fluctuations of the whole device caused by the local diffusion noise source can be represented as

$$s(x, \omega) = A e^2 n(x) S_v(x, \omega) |\nabla Z(x, \omega)|^2, \quad (23)$$

where $S_v(x, \omega)$ is the local spectral density of velocity fluctuations. Here it is implicitly assumed that noise sources located at different points are uncorrelated; the effect of spa-

tial correlation is widely discussed in Refs. 57–59. With this noise source the impedance field formula becomes

$$\begin{aligned} S_U(\omega) &= \int_0^L s(x, \omega) dx \\ &= A e^2 \int_0^L n(x) |\nabla Z(x, \omega)|^2 S_v(x, \omega) dx. \end{aligned} \quad (24)$$

It should be underlined that, as shown in Refs. 60–62, the spectral density of velocity fluctuations in bulk materials can be determined in terms of the same five parameters of the HD model by linearizing the corresponding balance equations [i.e., Eqs. (6) and (7) written for homogeneous case]. Since all the parameters of the HD Eqs. (6) and (7) depend only on the instantaneous local mean energy, it is reasonable to further suppose that in Eqs. (23)–(24) the spatial dependence of S_v is defined by the spatial dependence of the mean energy. Accordingly, $S_v(x)$ is the value of S_v calculated by MCP for bulk material at the same mean energy. Such an assumption closes the problem of noise calculations in the framework of the HD approach, since all quantities in Eq. (24), namely, the carrier concentration, the impedance field and the noise source are obtained from the same system of Eqs. (4)–(7). Moreover, the knowledge of the small-signal impedance $Z(\omega)$, also obtained in the framework of the same closed system by using the procedures described in Sec. II B, allows us to analyze the noise behavior when the structure is placed into a given external circuit. For example, the spectral density of the total current fluctuations, $S_J(\omega)$, induced by the structure when loaded by an external impedance $Z_{\text{load}}(\omega)$ takes the form

$$S_J(\omega) = \frac{S_U(\omega)}{|Z(\omega) + Z_{\text{load}}(\omega)|^2}. \quad (25)$$

When the spectral density of conduction-current fluctuations of the structure alone is of interest, Eq. (25) recovers the well-known relation:

$$S_J(\omega) = \frac{S_U(\omega)}{|Z(\omega)|^2}. \quad (26)$$

III. RESULTS AND DISCUSSION

The theory developed in the previous section is here applied to the case of GaAs n^+nn^+ diodes at $T_0 = 300$ K and compared with self-consistent MCP simulations for the purpose of validation. The numerical simulations are performed mainly for a submicron diode with the following parameters: the doping levels are $n = 5 \times 10^{15}$ and $n^+ = 10^{17} \text{ cm}^{-3}$, the cathode, n region, and anode lengths are respectively 0.3, 0.6, and 0.4 μm . Abrupt homojunctions are assumed. For the MCP simulations, usual values for the spatial mesh and time step are of 10 nm and 10 fs, respectively, and local boundary conditions are taken. These correspond to Ohmic contacts, i.e., neutrality in first and last meshes is achieved by injecting the necessary number of particles at the end of each time step according to a velocity weighted hemi-Maxwellian at thermal equilibrium.⁶³ For the HD simulations, values for the spatial mesh and time step are smaller than in the case of

MCP for a factor of 10, and Newmann boundary conditions are used for carrier concentration, velocity, and energy. To compare the behaviors of short and long diodes, some calculations have been performed for a long 1.25-7.5-1.25 μm n^+nn^+ diode with $n^+ = 2 \times 10^{16}$ and two different carrier concentrations in the n region: $n = 2 \times 10^{14}$ and $n = 10^{15} \text{ cm}^{-3}$. With the lower concentration the diode remains stable at high applied voltages (amplifying structure). With the higher concentration the diode exhibits self-oscillations for applied voltages above $U_{\text{th}} = 3.1$ V. To separate Ohmic behavior from hot-electron effects we firstly consider the case of near-equilibrium conditions.

A. Near-equilibrium conditions

We start our analysis with a simple analytical model which describes the behavior of both global and local perturbations in homogeneous resistors under thermal equilibrium, since the most general features of the electric field response can be already obtained at this level. By assuming that under thermal equilibrium conditions $n(x) = N_d(x)$, $E(x) = 0$, $v(x) = 0$, and neglecting energy perturbations, the system of Eqs. (4)–(6) can be linearized with respect to perturbations in the form

$$\delta n(x, t) = \frac{\epsilon \epsilon_0}{e} \frac{\partial \delta E(x, t)}{\partial x}, \quad (27)$$

$$\frac{\partial \delta E}{\partial t} + \frac{e}{\epsilon \epsilon_0} \delta v N_d = 0, \quad (28)$$

$$\frac{\partial \delta v}{\partial t} = e m^{-1} \delta E - \delta v \nu_v - \frac{Q_v}{N_d} \frac{\partial \delta n}{\partial x}. \quad (29)$$

Substitution of δn and δv from Eqs. (27) and (28), respectively, into Eq. (29) gives

$$\frac{\partial^2 \delta E}{\partial t^2} + \nu_v \frac{\partial \delta E}{\partial t} + \omega_p^2 \delta E = \nu_D^2 \frac{\partial^2 \delta E}{\partial x^2}, \quad (30)$$

where $\omega_p = (e^2 N_d / \epsilon \epsilon_0 m)^{1/2}$ is the plasma frequency and $\nu_D^2 = \langle \delta v^2 \rangle_0$ a square average thermal velocity associated with the variance of velocity fluctuations. Let us stress that at thermal equilibrium this velocity is strictly related to the diffusion process, since for $v = 0$, one has [see Eqs. (39)–(41) from Ref. 56] $\langle \delta v^2 \rangle_0 = D \tau_v$, where D is the diffusion constant and $\tau_v = 1/\nu_v$ the velocity relaxation time. For a homogeneous global perturbation, the right-hand side of Eq. (30) is equal to zero, and the left-hand side of Eq. (30) describes the time behavior of the perturbation. By assuming that the solution is proportional to $\exp(-\nu_v t)$, one obtains the square equation for the relaxation rates. For low doping levels, when $\nu_v > 2\omega_p$, the relaxation process is determined by two real values for the roots giving the relaxation times. For high doping levels, when $\nu_v < 2\omega_p$, the roots become complex and damped plasma oscillations appear. For n -GaAs, the transition from real to complex roots takes place for concentrations above about a threshold value of $n = 10^{15} \text{ cm}^{-3}$. Furthermore, by assuming that similar conditions hold also for the homogeneous hot-carrier transport, the critical concentration necessary to observe plasma effects shifts to higher values since the velocity relaxation rate increases considerably

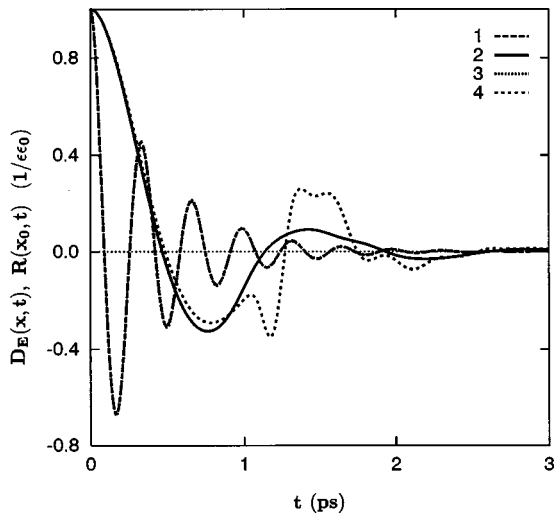


FIG. 1. Time dependence of the response functions at $J=0$ for the differential impedance (curves 1, 2) and the impedance field (curves 3, 4) calculated for points $x=0.1$ (curves 1, 3 which coincide) and $x=0.6$ (curves 2, 4) of the n^+ and n regions for the short diode, respectively.

with carrier heating. Thus, for carrier concentration below the threshold value one must observe only the relaxation, while above this value the relaxation is accompanied by plasma oscillations. Since at thermal equilibrium noise and small-signal characteristics satisfy Nyquist relation, the same time and frequency behavior must be observed also for the electronic noise.

For local perturbations introduced at a certain point of the structure, the right-hand side of Eq. (30) plays an essential role. Since the left-hand side remains the same, one can expect a similar time behavior also for the local perturbations. Furthermore, since both time and space derivatives are present, Eq. (30) describes also wave propagation. Due to the symmetry, one can expect the appearance of two waves propagating on opposite directions starting from the origin of the local perturbation. All the above features are illustrated by the results of the numerical HD modeling of the short diode presented below. Though the diode is a nonhomogeneous device consisting of three different regions, the independent features associated with each region are resembled in the results corresponding to the whole structure.

Figure 1 shows the time dependence of the local electric field response functions $D_E(x,t)$ calculated when $J=0$ for a global homogeneous perturbation of the total current in two points of the n^+ and n regions (curves 1 and 2, respectively) for the short diode. The damped oscillations are caused by plasma effects in these regions and are characterized by the corresponding plasma frequencies. Such a dependence is practically the same for all other points in these regions with exception of the areas which cover the homojunctions. Figure 1 also shows $R(x_0,t)$ calculated for the same points of the n^+ and n regions (curves 3 and 4, respectively). One can see that for the n^+ region curves 1 and 3 coincide entirely for both short and long time scales. For the n region $R(t)$ and $D_E(t)$ practically coincide only for the initial time interval $t < 1$ ps. A spatial integration of $D_E(x,t)$ over the whole structure gives the voltage response function, $D_U(t)$ shown

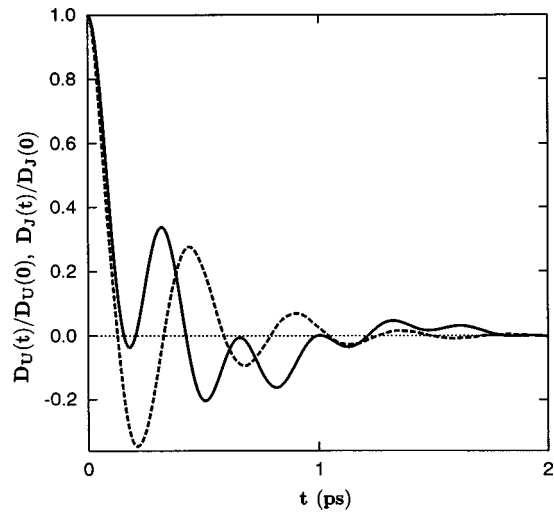


FIG. 2. Time dependence of the response functions of the voltage drop U (solid line) and the conduction current J (dashed line) of the short diode. Both functions are normalized to unity.

in Fig. 2 by the solid line. One can detect a linear superposition of two plasma oscillations since, due to the integration, each region provides separate contributions to $D_U(t)$. For completeness Fig. 2 also shows the conduction-current response function $D_J(t)$. Figure 3 presents the real part of the small-signal impedance of the whole structure, $\text{Re}[Z(f)]$, obtained by Fourier transformation of the voltage response function presented in Fig. 2. The plasma oscillations in the n and n^+ regions are responsible for two peaks of $\text{Re}[Z(f)]$ at frequencies independent of the region lengths and corresponding just to the plasma frequencies of these regions. The amplitude of each peak is proportional to the length of the corresponding region. By using the standard relation $Y(f) = 1/Z(f)$ one can also calculate the small-signal admittance of the structure. For comparison, Fig. 3 shows also $\text{Re}[Y(f)]$, which exhibits only one peak in the high-frequency region at an intermediate plasma frequency given by Eq. (3) of Ref. 64. The inverse Fourier transformation of $Y(f)$ yields the

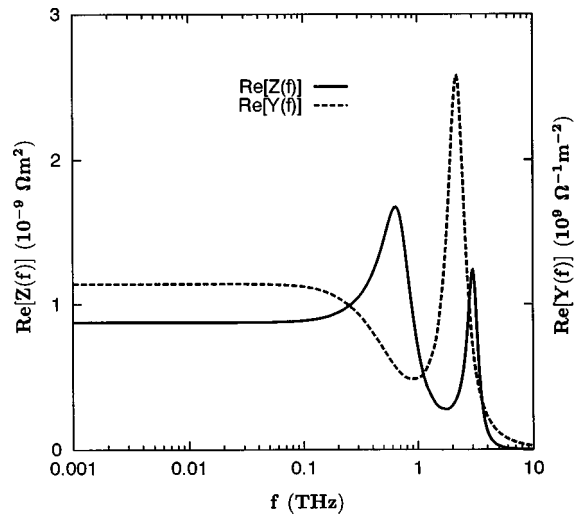


FIG. 3. Spectral dependence of the real part of the small-signal impedance and admittance of the short diode at thermal equilibrium.

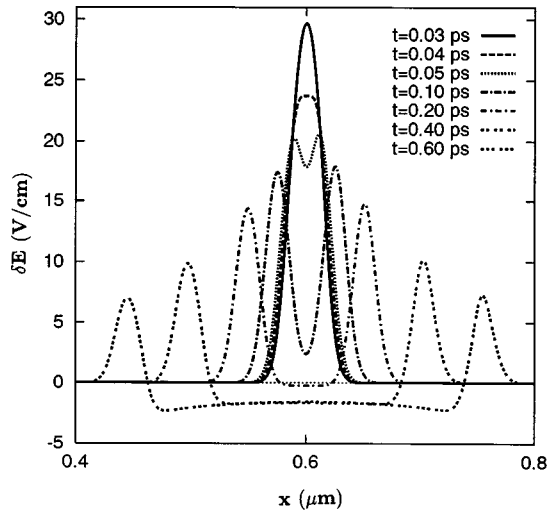


FIG. 4. Spatial profiles of the electric field perturbation at successive time moments of the short diode for an initial perturbation of Gaussian shape placed at point $x=0.6 \mu\text{m}$ of a $0.3\text{--}0.6\text{--}0.4 \mu\text{m } n^+nn^+$ GaAs structure.

response function of the conduction current, $D_J(t)$, shown in Fig. 2 by the dashed line. It should be underlined that due to Nyquist relation, $D_U(t)$ and $D_J(t)$ multiplied by $4k_B T_0$ (k_B being the Boltzmann constant and T_0 the bath temperature) give the autocorrelation functions of voltage and conduction current fluctuations at thermal equilibrium, respectively. Similarly, $\text{Re}[Z(f)]$ and $\text{Re}[Y(f)]$ multiplied by $4k_B T_0$ give the spectral densities of voltage and current noise. Therefore, under Ohmic conditions the main result is in the appearance of plasma peaks and plasma oscillations on, respectively, the spectral densities and correlation functions of fluctuating quantities.

Figure 4 shows the spatio-temporal evolution of a narrow Gaussian perturbation of the electric field δE induced at the initial time $t=0$ in the point $x=0.6 \mu\text{m}$ for $J=0$. During the first 20–30 fs the initial perturbation decreases and then it splits into two peaks which continue decreasing, while moving towards opposite sides with the same absolute velocity $v_D = (\langle \delta v^2 \rangle_0)^{1/2}$ given by the variance of velocity fluctuations. To a major extent, this can be associated with the diffusion process, since at thermal equilibrium v_D is strictly related to the diffusion coefficient D through the relation $v_D = (D\tau_v)^{1/2}$. Furthermore, one can interpret the propagation of the left and right peaks as a diffusive broadening of the initial Gaussian perturbation in the real space. However, the central part of the perturbation no longer keeps a Gaussian shape, rather it exhibits a complicate spatio-temporal behavior.

The electric field perturbations inside the structure lead to perturbations of the voltage drop U between the diode terminals. The time dependence of this perturbation is characterized by the impedance-field response function $R(x_0, t)$ defined by Eqs. (20) and (21), which describe the total response of the voltage to a local perturbation of conduction current. Let us recall that the differential-impedance response function $D_E(x, t)$ defined by Eq. (9) describes the local response of the electric field to a total current perturbation. The Fourier transformation of these functions gives the imped-

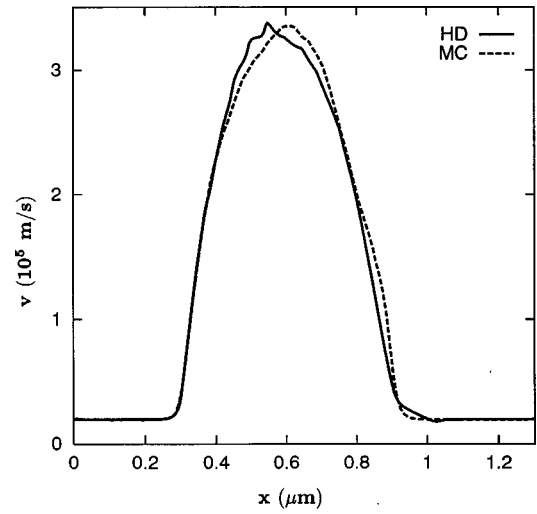


FIG. 5. Spatial profile of the average velocity of the short diode calculated for $U=0.6 \text{ V}$ by the HD and MCP approaches.

ance field and differential impedance, respectively. In Ref. 43 it was assumed that at thermal equilibrium they must coincide at least under nearly homogeneous conditions. Indeed, our calculations for the long diodes confirm this assumption. When we have compared these quantities in submicron structures, for the case of the n^+ region, we have found complete agreement in the whole time range while, for the n region, the agreement is limited to the short time scale $t < 1 \text{ ps}$. By comparing Fig. 1 with Fig. 4 we conclude that during the initial time-interval the electric field perturbation remains inside the n region. Then, when the right and left peaks of δE enter into the n^+ regions, $R(t)$ and $D_E(t)$ differ significantly. Thus, in submicron devices when the distance between the starting and ending points of the perturbation is comparable with the characteristic lengths of the structure, the differential impedance no longer coincides with the impedance field even at thermal equilibrium.

B. Small-signal, high-field characteristics

When the applied voltage or the total current flowing through the diode increases up to the onset for hot-carrier conditions the carrier dynamics becomes strongly inhomogeneous in a submicron structure. This is illustrated by Fig. 5, where the spatial profile of the average velocity calculated by HD and MC approaches is presented (solid and dashed curves, respectively). Thermal electrons coming from the cathode n^+ region (left contact) are sharply accelerated in the near-cathode area of the n region ($x=0.3\text{--}0.5 \mu\text{m}$) leading to a velocity overshoot followed by a monotonous decrease of the velocity up to the anode contact (right contact). Due to the negative slope of the velocity with respect to the spatial coordinate in most of the near-anode n region ($x=0.5\text{--}0.9 \mu\text{m}$), a given perturbation of carrier concentration can grow in time while crossing this region so that an amplification effect can take place: i.e., there exists a spatial negative differential conductivity (SNDO). This is illustrated in Fig. 6, where the differential impedance response function, which by definition is the local electric field response

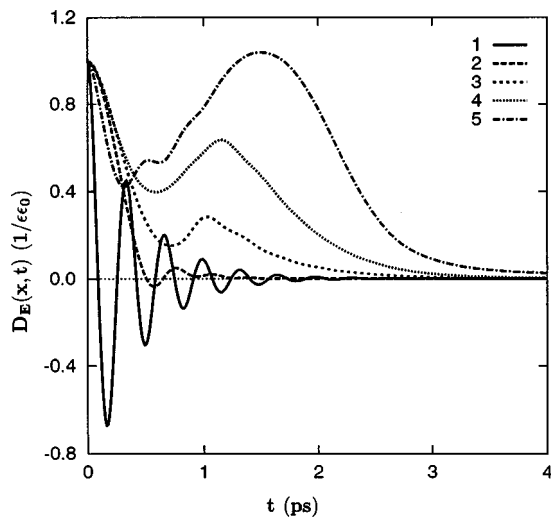


FIG. 6. Time dependence of the local electric field response of the short diode at points $x=0.1, 0.5, 0.7, 0.8, 0.9 \mu\text{m}$ (curves 1–5) to a global perturbation of the total current. $U=0.6 \text{ V}$.

$\delta E(x,t)/\delta E_0$ to a global perturbation of the total current, is presented. Curves 1 to 5 correspond respectively to $x=0.1, 0.5, 0.7, 0.8, 0.9 \mu\text{m}$. For the contacts, where the conditions are close to thermal equilibrium, the time dependence of $D_E(x,t)$ is similar to that already reported in Fig. 1. For the points placed in the n region, the initial part of $D_E(x,t)$ at $t < 0.3\text{--}0.5 \text{ ps}$ is also similar to that at thermal equilibrium (see curve 2 in Fig. 1) and is caused by the local processes responsible for a damping of the local electric field perturbation. However, for the points belonging to the negative slope of the average velocity (curves 3–5) a bell-shape tail appears with a maximum more pronounced the closer the point is to the end of the n region. The nature of this maximum was already discussed in detail in Refs. 54,65 for the case of an InP diode. It originates from the formation and further propagation across the active region of a secondary perturbation of the electron concentration and, hence, of the electric field, which grows while approaching the anode and then disappears inside the anode contact. The time at which the bell shape of $D_E(x,t)$ attains its maximum practically corresponds to the time when the secondary perturbation reaches the point x .

In accordance with Eq. (10) the Fourier transformation of $D_E(x,t)$ provides the local differential impedance in point x . The spatial profiles of the real part of the differential impedance calculated for frequencies $f=0, 100, 200, 300, 400 \text{ GHz}$ are presented in Fig. 7 (curves 1–5). For frequencies in the range $f=200\text{--}400 \text{ GHz}$, $\text{Re}[\nabla Z'(f,x)]$ is negative in the near-anode region of the n region. Thus, this region can amplify perturbations which cross it with a corresponding transit time of about 3 ps. In accordance with Eq. (13), the integration of the differential impedance throughout the structure gives the small-signal impedance of the whole device. The real and imaginary parts of $Z(f)$ are shown in Fig. 8. By comparing with Fig. 3 one can conclude that here the most significant difference appears in the low-frequency range. First of all, we find an increase for a about a factor of 5 of the low-frequency resistance which reflects the nonlin-

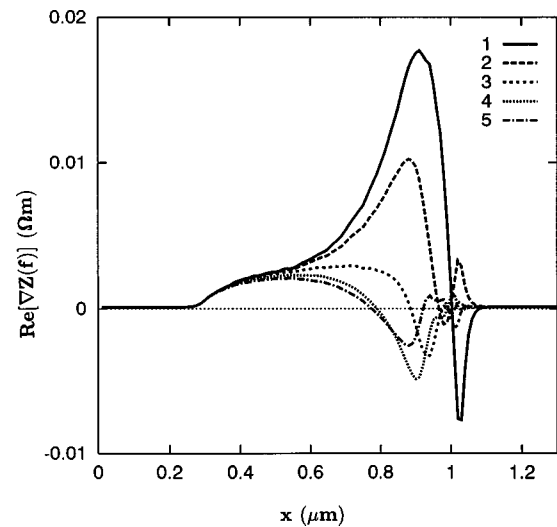


FIG. 7. Spatial profiles of the real part of the local differential impedance of the short diode calculated for frequencies respectively of $f=0, 100, 200, 300, 400 \text{ GHz}$ (curves 1–5).

ear shape of the current–voltage characteristic. The second feature is connected with the appearance of an additional minimum of $\text{Re}[Z(f)]$ at the frequency $f \approx 300 \text{ GHz}$ around which the amplification in the active region of the diode becomes possible. Nevertheless, the whole device still remains passive since $\text{Re}[Z(f)] > 0$ in the whole frequency range.

C. Transfer-impedance and impedance-field characteristics

For applied voltages sufficiently high for hot-carrier conditions to prevail, drift and transit-time effects have a significant influence on the evolution of local single perturbations. Accordingly, for the case of long diodes we assist to the appearance of transit-time dynamics of fluctuations as illustrated in Fig. 9. Here, the spatio-temporal evolution of an initial perturbation placed in the point $x=4.5 \mu\text{m}$ of the

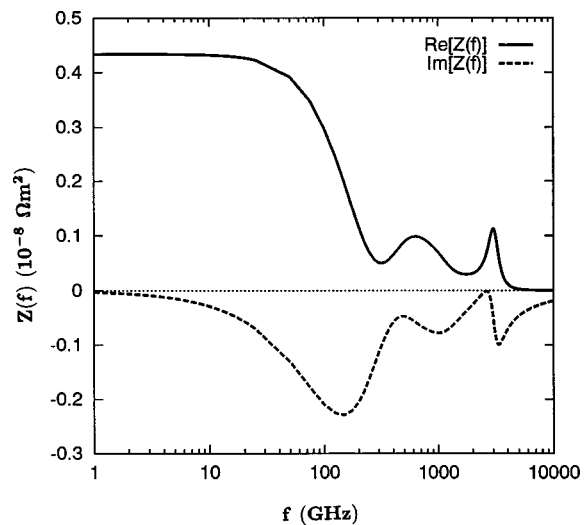


FIG. 8. Frequency dependence of the real and imaginary parts of the small-signal impedance of the short diode at $U=0.6 \text{ V}$.

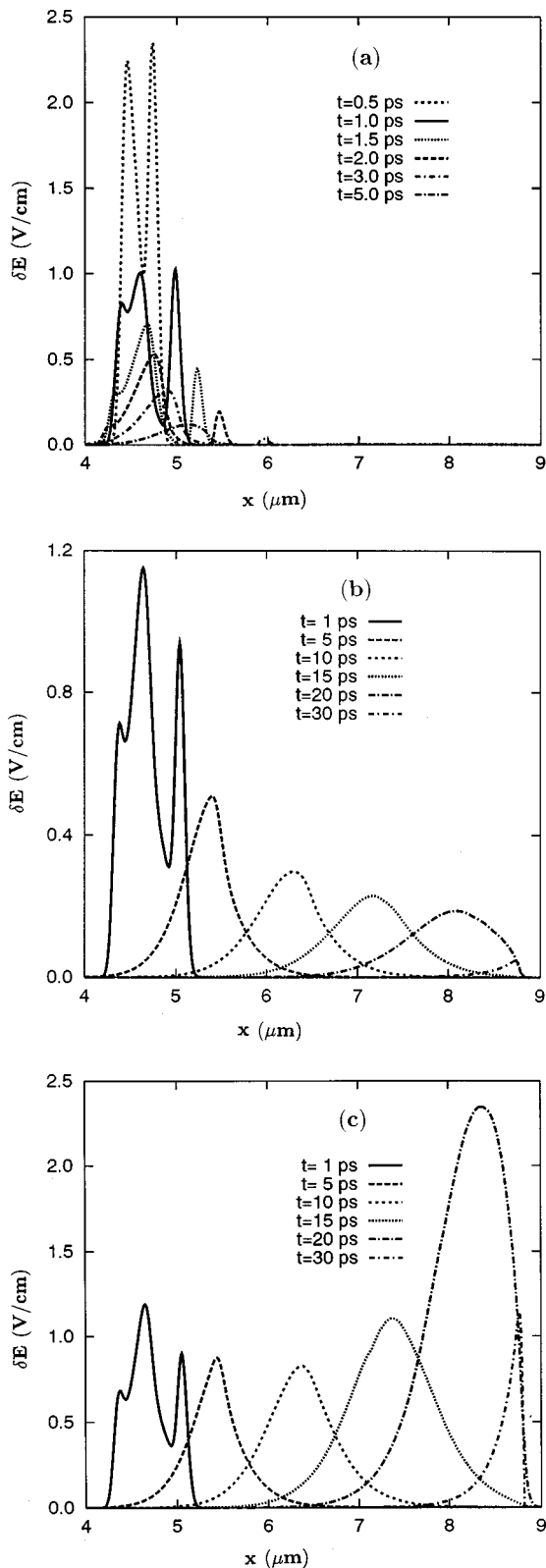


FIG. 9. Spatial profiles of the electric field perturbation at successive time moments calculated for the long diode with $n=10^{15} \text{ cm}^{-3}$ for an initial perturbation placed at $x=4.5 \mu\text{m}$, and different voltage drops. (a) $U=1.88$, (b) $U=2.6$, and (c) $U=3.05 \text{ V}$.

structure with $n=10^{15} \text{ cm}^{-3}$ is shown for increasing applied voltages of: (a) $U=1.88$, (b) $U=2.6$, and (c) $U=3.05 \text{ V}$. The primary stage of the evolution is quite similar for all voltages. Due to the relaxation character of the evolution for

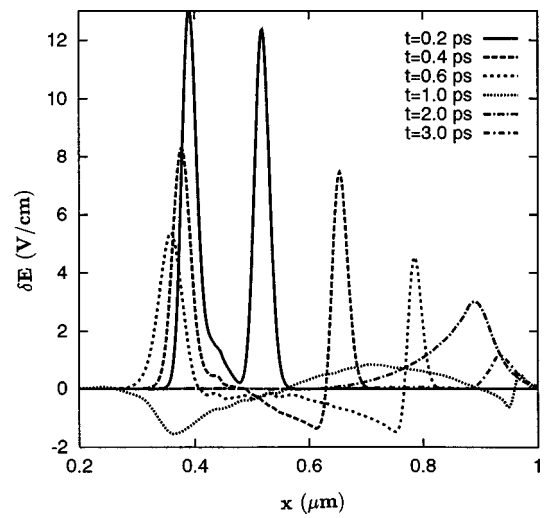


FIG. 10. Spatial profiles of the electric field perturbation at successive time moments calculated with $U=0.6 \text{ V}$ for an initial perturbation placed at $x=0.4 \mu\text{m}$ of the same short diode of Fig. 1.

low concentrations [see discussion of Eq. (30)], the perturbation decreases smoothly down to zero. Therefore, the negative values usual for oscillating behavior do not appear at all. In the meantime the right and left peak waves are separated from the initial perturbation, then start to move in opposite directions [see Fig. 9(a)], and finally, fastly vanishes (during the first 3–5 ps) at all applied voltages. The further evolution of the central peak strongly depends on the sign of the local differential impedance in the drift region. When the structure is locally passive in all points, the central peak moves towards the anode and vanishes after 5–10 ps [see Fig. 9(a)]. In this case, the time evolution of the perturbation is practically the same for all possible initial points in the n region. Furthermore, calculations show that in this case the impedance field coincides with the differential impedance. With a further increase of the voltage the damping decreases, so that the perturbation can already reach the anode contact [Fig. 9(b)]. By approaching the threshold voltage $U_{th}=3.1 \text{ V}$, the local amplification appears near the anode region. Therefore, the perturbation grows while moving through the active region and finally vanishes at the anode [Fig. 9(c)].

A similar evolution takes place also for submicron structures. The two main differences are that: (i) due to the high doping levels usual in these devices, the initial evolution of the central part of the perturbation exhibits a damped-oscillation scenario; (ii) due to the small transit distance the perturbation usually reaches the anode even in the absence of amplification, hence, to some extent transit-time effects are always present. This is illustrated in Fig. 10 where the spatio-temporal evolution of an initial perturbation placed at point $x=0.4 \mu\text{m}$ is shown for $U=0.6 \text{ V}$. In the first stage we observe the splitting of the initial perturbation into two peaks which move with velocities determined approximately by the combination of drift and diffusion velocities as $v=v_d \pm v_D$ (curves for $t < 1 \text{ ps}$). Such a behavior is similar to that already observed at thermal equilibrium. During this stage the central part of the perturbation placed between the left and

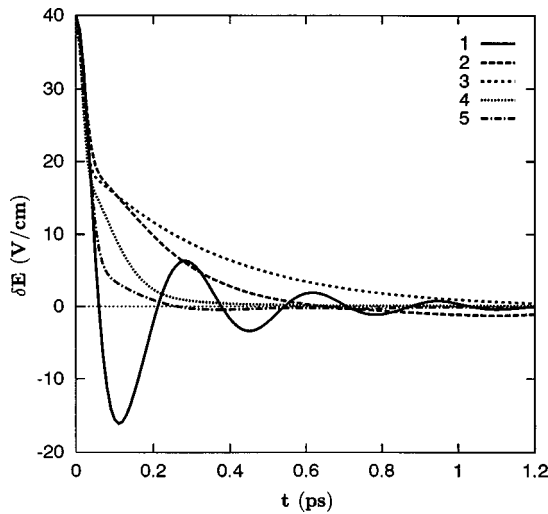


FIG. 11. Time dependence of the electric field response of the short diode in points $x' = 0.2, 0.4, 0.5, 0.7, 0.9 \mu\text{m}$ (respectively curves 1-5) for initial perturbations placed in the same points at $U = 0.6 \text{ V}$.

right peak waves oscillates in time and widens in space following the right peak up to the anode contact (Fig. 10, curves for $t > 1 \text{ ps}$). Then, the perturbation practically vanishes in all the points with positive differential impedance, while it grows in the region of local negative differential resistivity (curve for $t = 2 \text{ ps}$) which appears in the active region ($x = 0.8 - 1.1 \mu\text{m}$ for $U = 0.6 \text{ V}$) at frequencies of about 300 GHz, corresponding to the transit time throughout the active region (see Fig. 7). Finally, the perturbation disappears at the n^+ anode region (curve for $t = 3 \text{ ps}$).

For the short diode, the time dependence of the field response $\delta E(x, x'; t)$ in point x' due to an initial perturbation induced at point x of is shown in Figs. 11 and 12 for the diagonal ($x' = x$) and off-diagonal ($x' > x$) parts, respectively. The diagonal part exhibits plasma oscillations when the perturbation is placed at the contacts (Fig. 11, curve 1). For perturbations placed in the n region (curves 2-5) one

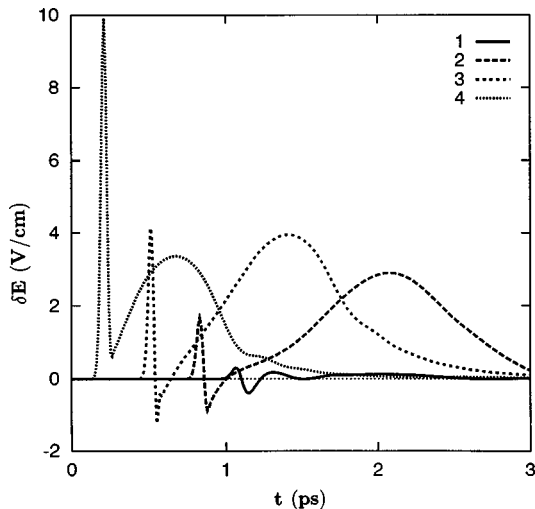


FIG. 12. Time dependence of the electric field response of the short diode in the point $x' = 0.9 \mu\text{m}$ for initial perturbations placed in points $x = 0.3, 0.4, 0.6, 0.8 \mu\text{m}$ (respectively curves 1-4) at $U = 0.6 \text{ V}$.

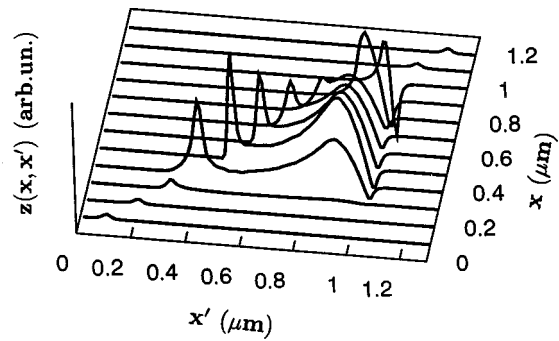


FIG. 13. Spatial dependence of the transfer-impedance matrix $z(x, x', f)$ of the short diode at frequency $f = 0$ and $U = 0.6 \text{ V}$.

can observe a sharp decrease at the shortest times ($t < 0.05 \text{ ps}$) similar to that of the n^+ region. The above sharp decrease is also caused by plasma processes and corresponds to the initial decrease of the primitive spike up to its splitting. A further time dependence of the local perturbation is connected with the spatio-temporal evolution of the left peak determined by the competition among diffusion, drift, and relaxation (see the behavior of the perturbation near the point $x = 0.4 \mu\text{m}$ shown in Fig. 10, which corresponds to curve 2 of Fig. 11). Figure 12 shows the time response of $\delta E(x, x'; t)$ in the point $x' = 0.9 \mu\text{m}$ i.e., at the end of the n region) for initial perturbations placed at points $x = 0.3, 0.4, 0.6, 0.8 \mu\text{m}$ (respectively curves 1-4). For the points placed in the n region, the time response evidences three time scales. The initial time scale is related to the delay time which is necessary for the right peak of δE (see Fig. 10) to reach the anode contact (during this time the response is equal to zero). The intermediate time-scale manifests itself as a sharp spike caused by the propagation of the right δE peak through the point x' . The final time scale corresponds to the propagation of the central part of the perturbation through the point x' and is associated with both the amplification of the perturbation in the active region and the transit-time effect.

Due to the various effects and the associated characteristic times, the spatial and spectral behavior of the transfer-impedance matrix $z(x, x', f)$ exhibits a rather complicated shape. As an example, Fig. 13 shows the spatial dependence of the static (i.e., $f = 0$) transfer impedance. The appearance of $\delta(x - x')$ -like spikes, which are more pronounced at the beginning of the n region, is related to the longest relaxation of the diagonal contribution of the field response (see Fig. 11). The broad peaks of $z(x, x', 0)$ appearing near the end of the n region are associated with transit-time effects.

The integration of the transfer impedance throughout the structure with respect to the coordinate x which labels the perturbation origin gives the differential impedance already considered in Sec. III B. However, let us underline, that for the calculation of the differential impedance it is better to use the direct procedure described in Sec. II B rather than the transfer-impedance integration.

The integration of the transfer impedance throughout the structure with respect to the coordinate x' which labels the perturbation observation gives the corresponding impedance field. The time dependence of the perturbation of the voltage

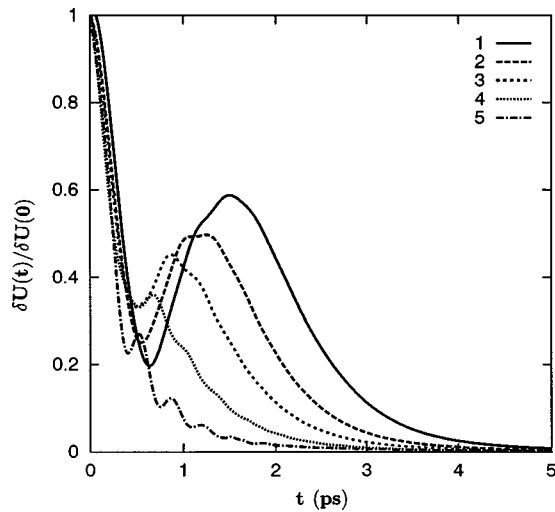


FIG. 14. Time dependence of the perturbation of the voltage drop between the short diode terminals for an initial perturbation of the electric field placed at points $x=0.475, 0.575, 0.675, 0.775,$ and $0.875 \mu\text{m}$ (respectively curves 1–5) at $U=0.6 \text{ V}$.

drop between the diode terminals for an initial perturbation of the electric field placed at different points of the structure is shown in Fig. 14. As usual, at initial times one can observe a monotonous decrease of the voltage perturbation caused by the initial relaxation of the local electric field perturbation and the quick damping of the splitted waves. Then, the formation, propagation, and disappearance of the central part of the perturbation leads to the bell-shaped evolution of the voltage perturbation in the longer time scale. This bell-shaped tail is similar to that observed in the case of the local electric field perturbation caused by the global perturbation of the total current. Of course, in both cases it is caused by the propagation and amplification of the perturbation in the region of the device which exhibits SNDC. The difference lies in the fact that $D_E(x,t)$ manifests the pronounced bell-shaped behavior at points x placed near the anode (where the perturbation is observed), while the similar shape of $R(x,t)$ takes place for points x near the cathode (where the perturbation is originated). When the origin of the initial perturbation is shifted toward the anode contact, the bell-shaped tail of the voltage perturbation becomes less pronounced (see Fig. 14, curves 2–4). If the plasma frequency is considerably higher than the damping rate of the splitted waves, then the splitted-wave propagation is accompanied by plasma oscillations. Such a situation is typical for perturbations placed in n^+ regions or nearby (see Fig. 14, curve 5). Figure 15 reports the high-frequency spectrum of $|\nabla Z(x;\omega)|^2$ calculated for initial perturbations placed at different points inside the n region of the short diode. The deviations from a simple Lorentzian decay in the cut-off region above 200 GHz reflect the effects of the transit time on the perturbation in the n region. As it follows from Fig. 15, such a transit-time effect has a resonant character leading to minima of $|\nabla Z(x;\omega)|^2$ at the corresponding frequencies. Due to this reason, the spatial profile of $|\nabla Z(x;\omega)|^2$ also manifests a minimum inside the n region in the frequency range $f=300\text{--}600 \text{ GHz}$. This is evidenced in Fig. 16 which shows the spatial dependence of the

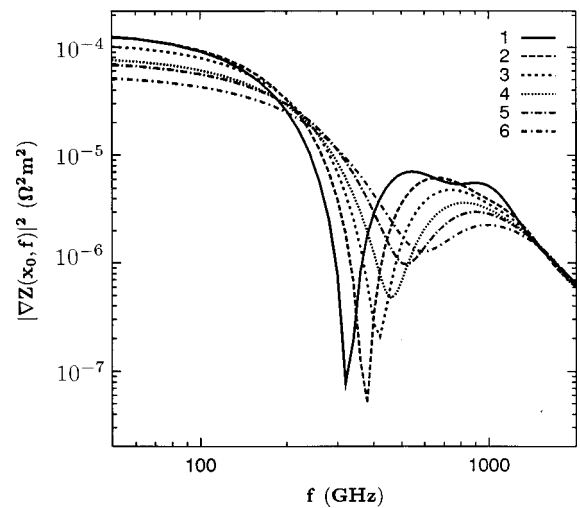


FIG. 15. Frequency dependence of the absolute value squared of the impedance field $|\nabla Z(x_0; \omega)|^2$ of the short diode calculated for initial perturbations placed at points $x=0.425, 0.475, 0.525, 0.575, 0.625,$ and $0.675 \mu\text{m}$ (respectively curves 1–6) at $U=0.6 \text{ V}$.

absolute value squared of the impedance field $|\nabla Z(x;\omega)|^2$ calculated at different frequencies.

D. Noise source

In the framework of the closed HD approach based on Eqs. (4)–(7) and Eq. (24) the diffusion noise is given by the spectral density of velocity fluctuations, $S_v(\omega)$, which can be directly calculated from the same model by linearizing the balance equations.^{60–62} The field and energy dependence of the spectral density of velocity fluctuations obtained in such a way are found to be in full qualitative and good (with an accuracy at worst of 20%) quantitative agreement with the $S_v(\omega)$ directly calculated by the MC approach.⁶⁶ The spatial profiles of the spectral density of velocity fluctuations calculated by the HD approach for the submicron diode are shown

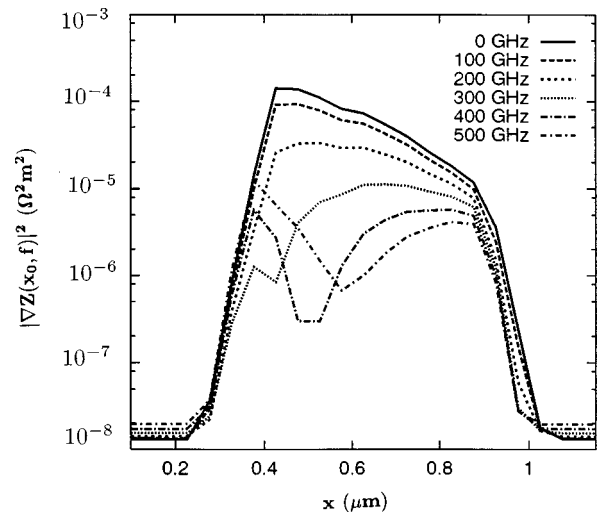


FIG. 16. Spatial profiles of the absolute value squared of the impedance field $|\nabla Z(x_0; \omega)|^2$ of the short diode calculated at different frequencies.

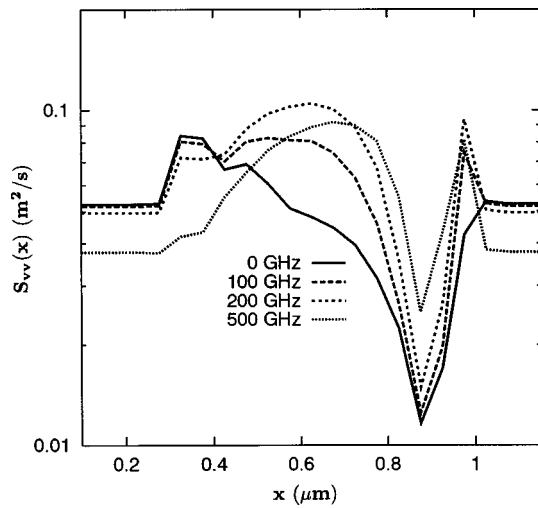


FIG. 17. Spatial profiles of the HD noise source of the short diode represented by the spectral density of velocity fluctuations calculated at different frequencies.

in Fig. 17 at different frequencies. The complicated behavior of $S_v(x, \omega)$ is determined by the frequency and field dependence of $S_v(\omega)$ in the bulk material.⁶⁶

E. Spectral density of voltage fluctuations

The local contribution of each point of the submicron structure, $s(x, f)$, to the spectral density of voltage fluctuations between the structure terminals, $S_U(f)$, calculated in accordance with Eq. (23) is shown in Fig. 18 for $f=0$ at $U=0$ and 0.6 V. For both voltages the main contribution comes from the n region. For $U=0$, as expected, this quantity is more or less homogeneously distributed along the n region, and exhibits spikes near the homojunctions due to the space charge at the interface. It should be stressed that in submicron structures, even at $U=0$, the typical dimensions of the perturbation propagation are comparable with the length of the structure (see Fig. 4). Therefore, due to the

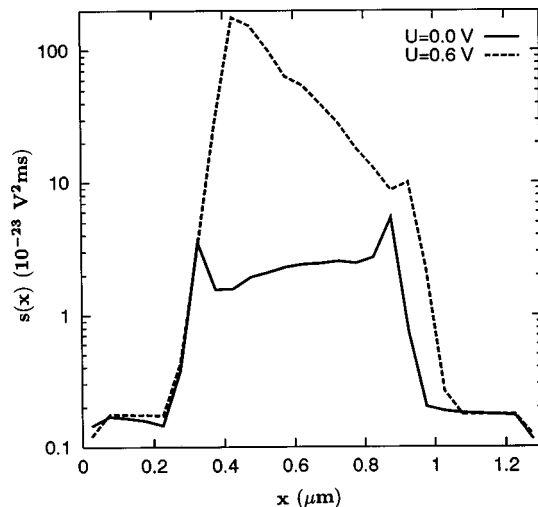


FIG. 18. Local contribution to the total voltage spectral density of the short diode at frequency $f=0$ for $U=0$ and 0.6 V (solid and dashed lines, respectively).

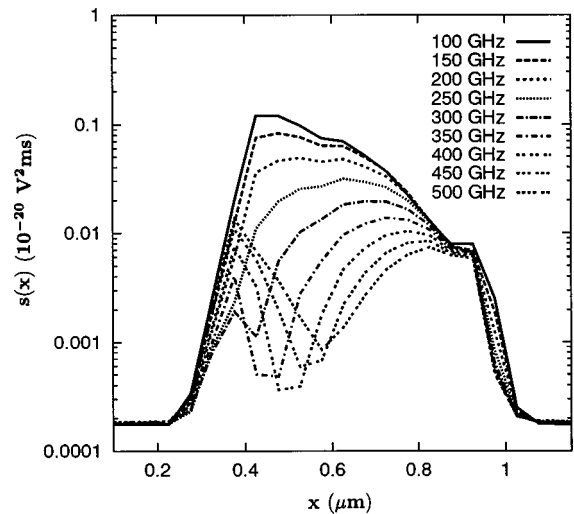


FIG. 19. Local contribution to the total voltage spectral density of the short diode at different frequencies for $U=0.6$ V.

asymmetry of the n^+ regions (the right contact is longer than the left one), different points in the n region give slightly different contributions to the total noise. This is reflected by the systematic increase of $s(x)$ while approaching the end of the n region. For $U=0.6$ V, $s(x, 0)$ exhibits a maximum near the beginning of the n region and monotonously decreases by approaching the anode where a penetration effect associated with the energy relaxation length of hot carriers takes place. In the thermal regions of the structure (near cathode and anode) the curves for $U=0$ and 0.6 V coincide. We conclude that in the presence of increasing voltages the most significant contribution to the total noise comes from the near-cathode area of the n region and this is mostly due to transit-time effects. Figure 19 shows the local contributions of different points of the diode to the total noise at different frequencies of interest. Again, in the frequency range corresponding to pronounced transit-time effects one can observe the occurrence of a minimum due to the resonant behavior of the local contributions to the noise. By comparing Figs. 16, 17, and 19 we conclude that both the general shape of the profiles and the details of the local contribution are caused mainly by the impedance field behavior. Indeed, the spatial variations of $|\nabla Z(x; \omega)|^2$ under hot-electron conditions are much stronger (about one to two orders in magnitude) than the variations of the spectral density of velocity fluctuations.

It should be underlined that, in the framework of the MCP approach, one can also obtain some kind of spatial map of the noise distribution throughout the structure. Usually this is represented by the spectral density of voltage fluctuations between the points 0 and x , $S_U(x, f)$.^{17,39} The same characteristic can also be calculated by the HD approach. For this sake, the voltage response at points x ($0 < x < L$) of the device is calculated in parallel with the voltage response between the structure terminals and the impedance field $\nabla Z_{0x}(x_0, f)$ corresponding to the voltage response between the points 0 and x due to a perturbation in point x_0 is obtained in the usual way from Fourier transformation of the response functions of the local voltage. The substitution of $\nabla Z_{0x}(x_0, f)$ in place of $\nabla Z(x, f)$ in Eq. (24) gives the spatial

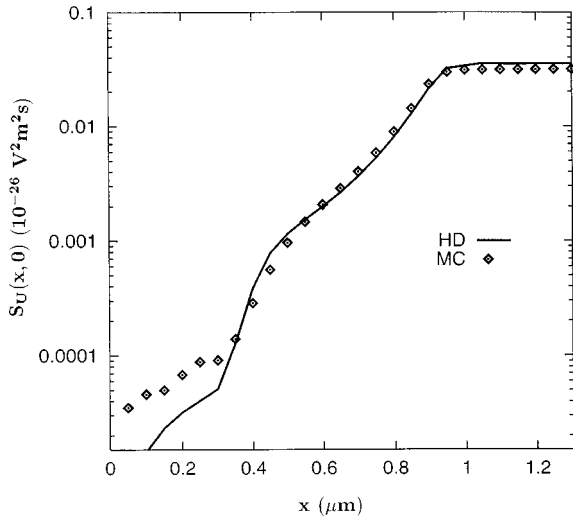


FIG. 20. Spatial dependence of the spectral density of voltage fluctuations $S_U(x, f)$ in the short diode of Fig. 1.

dependence of $S_U(x, f)$. Figure 20 presents the spatial dependence of $S_U(x, f)$ calculated by both MCP and HD approaches in the case of the short diode for $f=0$. The most significant increase of $S_U(x, 0)$ takes place in the near-anode area of the n region. Therefore, in spite of the fact that the noise is originated in the near-cathode region, it manifests itself near the near-anode region which is characterized by the higher resistance originated by hot-carrier effects.

Finally, Fig. 21 shows the spectral density of voltage fluctuations between the terminals of the short diode $S_U(f)$ calculated for $U=0$ (curves 1–3) and $U=0.6$ V (curves 4–6) in several ways: (i) at thermal equilibrium by using the small-signal impedance calculated by the HD approach and

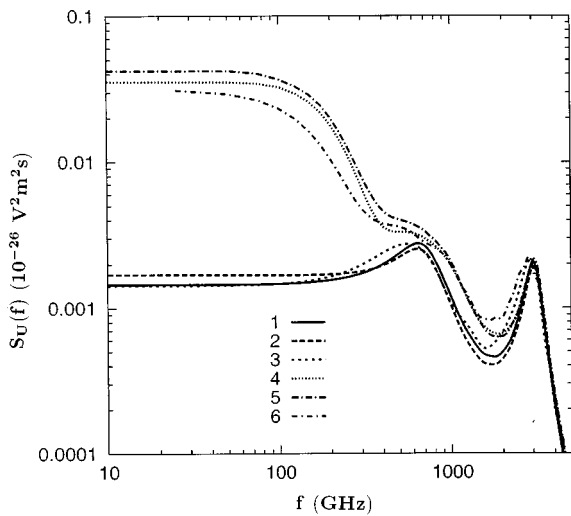


FIG. 21. Frequency dependence of the spectral density of voltage fluctuations in the short diode of Fig. 1 calculated at $U=0$ (curves 1–3) and $U=0.6$ V (curves 4–6) by using different techniques: (i) at thermal equilibrium by using the small signal impedance calculated by HD approach and Nyquist theorem (curve 1), (ii) by using the IF method according to Eq. (24) with the noise source calculated by the HD (curves 2 and 4) and MCP (curve 5) approaches, (iii) by using the direct MCP technique (curves 3 and 6).

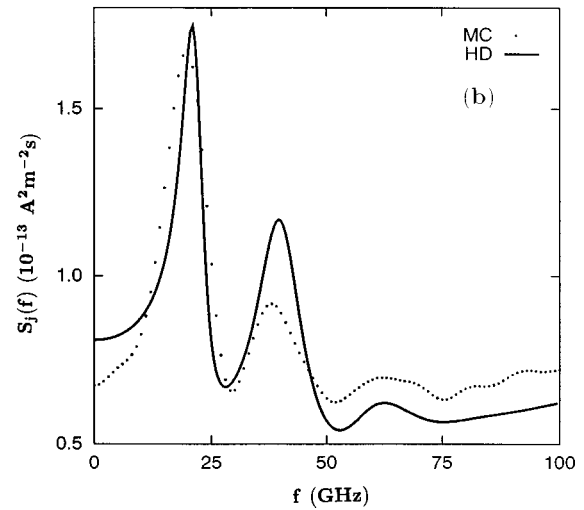
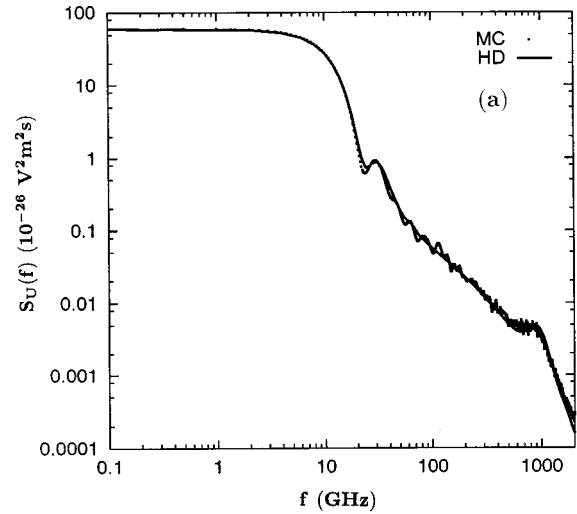


FIG. 22. Frequency dependence of the spectral densities of: (a) voltage and (b) conduction current fluctuations in the long diode with $n=2 \times 10^{14} \text{ cm}^{-3}$ calculated at $U=8$ V by the HD and MCP approaches (solid line and dots, respectively).

Nyquist theorem (curve 1), (ii) by using the impedance field method according to Eq. (24) with the local spectral density of velocity fluctuations calculated by the HD (curves 2 and 4) and the MCP (curve 5) approaches, and (iii) by using the direct MCP technique (curves 3 and 6). By naturally including all the processes responsible for the fluctuations and their correlations, the MCP technique is used here to validate the calculations performed with the impedance-field and transfer-impedance methods. The high-frequency region of the spectrum exhibits the plasma peak associated with the electrons in the n^+ contacts which remain thermal at any reasonable applied voltage. Therefore, here $S_U(f)$ is practically the same for both Ohmic and hot-electron conditions in the n region. By focusing on the low-frequency region of the spectrum, we can observe a considerable increase of the electronic noise under hot-electron conditions caused by transit-time effects. A similar behavior of the voltage noise spectra is observed for the long diodes as illustrated in Fig. 22(a). In both cases, the cutoff of the low-frequency plateau corresponds to the transit-time frequency equal to 20 and 300 GHz for the long and short structures, respectively. Let us

recall, that in accordance with Eqs. (25) and (26), the voltage noise spectra obtained by the HD approach can be used to calculate the spectral density of conduction current fluctuations, $S_j(f)$, as well as to analyze the noise in various circuits. As an example, Fig. 22(b) shows $S_j(f)$ (solid line) obtained from $S_U(f)$ [presented in Fig. 22(a)] by using Eq. (26). For comparison, the results of the direct simulation of $S_j(f)$ with the MCP method are shown by dots. The presence of the two resonant peaks is connected with two amplification bands appearing in the long structures under high applied voltage.

By comparing the different approaches illustrated in Figs. 20 and 22 one can conclude that they provide a full qualitative and good quantitative agreement for both over micron and submicron structures. This agreement validates the formalism of the impedance and transfer-impedance methods developed here, primarily for submicron structures, in the framework of the HD approach which considers the use of the energy-dependent spectral density of velocity fluctuations obtained from the balance equations as the local source of diffusion noise.

IV. CONCLUSIONS

In the framework of the transfer-impedance and impedance-field methods, we have developed a closed HD approach based on the velocity and energy conservation equations to calculate the small-signal and voltage-noise characteristics of two-terminal semiconductor structures. The approach has been applied to n^+nn^+ GaAs structures of overmicron and submicron length at $T_0=300$ K. The good agreement with the noise characteristics calculated with the MCP method validates the approach developed here whose main advantages can be summarized as follows:

(i) Once the input set of the material parameters are given, the approach operating at a hydrodynamic level is flexible, efficient, and sufficiently fast to enables modeling of different geometries, doping profiles, applied voltages, temperatures, and so on. Thus, we believe it represents an important step for the development of accurate and physically plausible simulators in modern deep submicron electronics.

(ii) All physical quantities related to the impedance field formulation of voltage noise, namely, the carrier concentration, the impedance, and differential impedance fields, and the local spectral density of velocity fluctuations, are calculated in the framework of the same microscopic model, thus providing a unified approach for the evaluation of the spectral density of voltage fluctuations of the global structure.

(iii) The small-signal impedance and the voltage spectral density of the structure under test are calculated by using the same approach thus allowing one to calculate the device noise temperature, to obtain the parameters of Thevenin and Norton generators, to analyze the noise behavior of the device in various external circuits, etc.

(iv) The time-domain representation at the basis of this approach allows one to trace a spatio-temporal evolution of a single perturbation placed at any point of the structure thus providing a local information about the main physical processes responsible for the device noise performance.

(v) Calculations of the local and global electrical response of the device under test allows one to obtain various local characteristics such as the transfer impedance, the local contribution to the noise, the spatial distribution of the noise spectrum, etc. thus providing a comprehensive spatial map of the device noise sources and their propagation.

(vi) For the structures here analyzed transit-time effects are found to influence substantially the noise spectra in a wide frequency range which extends above 10 GHz at decreasing length of the active region.

ACKNOWLEDGMENTS

This work has been performed within the Italian-Lithuanian Project "Research and Development Cooperation in Submicron Electronics" and supported by the Italian Ministry of Foreign Affairs. Partial support from the NATO networking linkage Grant HTECH.LG 960931, Computer Networking Supplement CNS 970627, Grant DRIC/MDLM/MT n. 1675 of Ministero de l'Education Nationale, de l'Enseignement Superieur, et de la Recherche, Grant PICASSO n.97090 of Ministero des Affaires Etrangeres, and project SA11/96 from the Consejeria de Cultura de la Junta de Castilla y León. is gratefully acknowledged.

¹ *High-Speed Semiconductor Devices*, edited by S. M. Sze (Wiley, New York, 1990).

² *Supercomputer Simulation of Semiconductor Devices*, edited by M. Shur and T. A. Fjeldy (North-Holland, Amsterdam, 1991).

³ P. J. Price, *Semicond. Semimet.* **14**, 249 (1979).

⁴ R. W. Hockney and J. W. Eastwood, *Computer Simulation Using Particles* (McGraw-Hill, New York, 1981).

⁵ C. Jacoboni and L. Reggiani, *Rev. Mod. Phys.* **55**, 645 (1983).

⁶ C. Jacoboni and P. Lugli, in *The Monte Carlo Method for Semiconductor Device Simulation*, edited by S. Selberherr, Springer Series in Computational Micro Electronics (Springer, Berlin, 1989).

⁷ M. V. Fischetti and S. E. Laux, *Phys. Rev. B* **38**, 9721 (1988).

⁸ J. Zimmermann and E. Constant, *Solid-State Electron.* **23**, 915 (1980).

⁹ B. Boittiaux, E. Constant, and A. Ghis, in *Noise in Physical Systems and 1/f Noise*, edited by M. Savelli, G. Lecoy, and J.-P. Nougier (Elsevier, Amsterdam, 1983), p. 19.

¹⁰ C. Moglestue, in *Noise in Physical Systems and 1/f Noise*, edited by M. Savelli, G. Lecoy, and J.-P. Nougier (Elsevier, Amsterdam, 1983), p. 23.

¹¹ C. Moglestue, *IEEE Trans. Electron Devices* **32**, 2092 (1985).

¹² B. R. Nag, S. R. Ahmed, and M. Deb Roy, *Appl. Phys. A* **41**, 197 (1986).

¹³ D. Junevičius and A. Reklaitis, *Electron. Lett.* **24**, 1307 (1988).

¹⁴ J. Gest, H. Fawaz, H. Kabbaj, and J. Zimmermann, in *Noise in Physical Systems and 1/f Fluctuations*, edited by T. Musha, S. Sato, and M. Yamamoto (Ohmsha, Kyoto, 1991), p. 291.

¹⁵ J. G. Adams and T.-W. Tang, *IEEE Electron Device Lett.* **13**, 378 (1992).

¹⁶ L. Varani, T. Kuhn, L. Reggiani, and Y. Perles, *Solid-State Electron.* **36**, 251 (1993).

¹⁷ T. Gonzalez, D. Pardo, L. Varani, and L. Reggiani, *Appl. Phys. Lett.* **63**, 84 (1993).

¹⁸ T. Gonzalez and D. Pardo, *J. Appl. Phys.* **73**, 7453 (1993).

¹⁹ T. Gonzalez, D. Pardo, L. Varani, and L. Reggiani, *Appl. Phys. Lett.* **63**, 3040 (1993).

²⁰ T. Gonzalez, D. Pardo, L. Varani, and L. Reggiani, in *ESSDERC'93*, edited by J. Borel, P. Gentil, J. P. Noblanc, A. Nouallhat, and M. Verdone (Frontieres, Gif-sur Yvette, 1993), p. 3040.

²¹ K. Y. Lee, H. S. Min, and Y. J. Park, *Solid-State Electron.* **36**, 1563 (1993).

²² V. Gruzinskis, V. Mitin, E. Starikov, and P. Shiktorov, *J. Appl. Phys.* **75**, 935 (1994).

²³ V. Gruzinskis, E. Starikov, P. Shiktorov, R. Gričius, V. Mitin, L. Reggiani, and L. Varani, *Proceedings European Gallium Arsenide and Related III-V Compounds Applications Symposium, Politecnico di Torino, Italy, April 28-30, 1994*, p. 365.

- ²⁴ V. Gruzinskiis, V. Mitin, E. Starikov, and P. Shiktorov, *J. Appl. Phys.* **75**, 8210 (1994).
- ²⁵ J. G. Adams, T.-W. Tang, and L. E. Kay, *IEEE Trans. Electron Devices* **41**, 575 (1994).
- ²⁶ T. Gonzalez, D. Pardo, L. Varani, and L. Reggiani, *IEEE Trans. Electron Devices* **42**, 991 (1995).
- ²⁷ V. Gruzinskiis, E. Starikov, and P. Shiktorov, *Phys. Scr.* **T54**, 146 (1994).
- ²⁸ V. Gruzinskiis, E. Starikov, P. Shiktorov, R. Gričius, V. Mitin, L. Reggiani, and L. Varani, *Semicond. Sci. Technol.* **9**, 1843 (1994).
- ²⁹ L. Varani, L. Reggiani, T. Kuhn, T. Gonzalez, and D. Pardo, *IEEE Trans. Electron Devices* **41**, 1916 (1994).
- ³⁰ V. Gruzinskiis, E. Starikov, P. Shiktorov, L. Reggiani, L. Varani, J. C. Vaissiere, J. P. Nougier, P. Houlet, and L. Hlou, in *Proceedings of the 7th Vilnius Conference on Fluctuation Phenomena in Physical Systems, Palanga, Lithuania, Oct. 4-7, 1994*, edited by V. Palenskis (Vilnius University, Palanga, 1994), p. 205.
- ³¹ V. Gruzinskiis, E. Starikov, P. Shiktorov, V. Mitin, L. Reggiani, L. Varani, J. C. Vaissiere, J. P. Nougier, P. Houlet, L. Hlou, and D. Gasquet, in *Proceedings of the 7th Vilnius Conference on Fluctuation Phenomena in Physical Systems, Palanga, Lithuania, Oct. 4-7, 1994*, edited by V. Palenskis (Vilnius University, Palanga, 1994), p. 211.
- ³² E. Starikov, P. Shiktorov, V. Gruzinskiis, J. P. Nougier, J. C. Vaissiere, L. Varani, and L. Reggiani, *Appl. Phys. Lett.* **66**, 2361 (1995).
- ³³ V. Gruzinskiis, E. Starikov, P. Shiktorov, L. Reggiani, and L. Varani, in *Proceedings of the 13th International Conference on Noise in Physical Systems and 1/f Fluctuations, Palanga, Lithuania, May 29-June 3, 1995*, edited by V. Bareikis and R. Katilius (World Scientific, Singapore, 1995), p. 177.
- ³⁴ V. Gruzinskiis, E. Starikov, P. Shiktorov, L. Reggiani, J. C. Vaissiere, J. P. Nougier, L. Varani, P. Houlet, and D. Gasquet, in *Proceedings of the 13th International Conference on Noise in Physical Systems and 1/f Fluctuations, Palanga, Lithuania, May 29-June 3, 1995*, edited by V. Bareikis and R. Katilius (World Scientific, Singapore, 1995), p. 189.
- ³⁵ V. Gruzinskiis, E. Starikov, and P. Shiktorov, *Lith. Phys. J.* **35**, 445 (1995).
- ³⁶ E. Starikov, P. Shiktorov, V. Gruzinskiis, J. P. Nougier, J. C. Vaissiere, L. Varani, and L. Reggiani, *J. Appl. Phys.* **79**, 242 (1996).
- ³⁷ E. Starikov, P. Shiktorov, V. Gruzinskiis, T. Gonzalez, M. J. Martin, D. Pardo, L. Reggiani, and L. Varani, *Semicond. Sci. Technol.* **11**, 865 (1996).
- ³⁸ P. Shiktorov, V. Gruzinskiis, E. Starikov, L. Reggiani, and L. Varani, *Phys. Rev. B* **54**, 8821 (1996).
- ³⁹ L. Reggiani, P. Golinelli, L. Varani, T. Gonzalez, D. Pardo, E. Starikov, P. Shiktorov, and V. Gruzinskiis, *Microelectron. J.* **28**, 183 (1997).
- ⁴⁰ L. Reggiani, E. Starikov, P. Shiktorov, V. Gruzinskiis, and L. Varani, *Semicond. Sci. Technol.* **12**, 141 (1997).
- ⁴¹ W. Schokley, J. A. Copeland, and R. P. James, in *Quantum Theory of Atoms, Molecules and Solid State*, edited by P. O. Lowdin (Academic, New York, 1966), p. 537.
- ⁴² K. M. van Vliet, A. Friedman, R. J. J. Zijlstra, A. Gisolf, and A. Van der Ziel, *J. Appl. Phys.* **46**, 1804 (1975); **46**, 1814 (1975).
- ⁴³ J. P. Nougier, J. C. Vaissiere, D. Gasquet, and A. Motadid, *J. Appl. Phys.* **52**, 5683 (1981).
- ⁴⁴ J. P. Nougier, A. Moatadid, J. C. Vaissiere, and D. Gasquet, *Physica* **134B**, 260 (1985).
- ⁴⁵ J. P. Nougier, A. Moatadid, J. C. Vaissiere, and D. Gasquet, *Noise in Physical Systems and 1/f Noise-1985* (Elsevier, Amsterdam, 1986), p. 105.
- ⁴⁶ G. Ghione, ESSDERC'90 (IOP, Nottingham, 1990), p. 225.
- ⁴⁷ F. Filicori, G. Ghione, and C. U. Naldi, *IEEE Trans. Microwave Theory Tech.* **40**, 1333 (1992).
- ⁴⁸ G. Ghione and F. Filicori, *IEEE Trans. Comput.-Aided Des.* **12**, 425 (1993).
- ⁴⁹ H. U. Baranger and J. W. Wilkins, *Phys. Rev. B* **36**, 1487 (1987).
- ⁵⁰ G. Baccarani, M. Rudan, R. Guerrieri, and P. Ciampolini, in *Advances in CAD for VLSI, Vol 1: Process and Device Modeling*, edited by W. L. Engl (North Holland, New York, 1986), p. 107.
- ⁵¹ H. L. Grubin, in *The Physics of Submicron Semiconductor Devices*, edited by H. L. Grubin, D. K. Ferry, and C. Jacoboni (Plenum, New York, 1988), p. 45.
- ⁵² D. L. Woolard, H. Tian, R. J. Trew, M. A. Littlejohn, and K. W. Kim, *Phys. Rev. B* **44**, 11119 (1991).
- ⁵³ M. Nekovee, B. J. Geurts, H. M. J. Boots, and M. F. H. Schuurmans, *Phys. Rev. B* **45**, 6643 (1992).
- ⁵⁴ V. Gruzinskiis, E. Starikov, P. Shiktorov, L. Reggiani, and L. Varani, *Phys. Rev. B* **49**, 13650 (1994).
- ⁵⁵ V. Gruzinskiis, E. Starikov, P. Shiktorov, L. Reggiani, and L. Varani, *J. Appl. Phys.* **76**, 5260 (1994).
- ⁵⁶ V. Gruzinskiis, E. Starikov, and P. Shiktorov, *Solid-State Electron.* **36**, 1055 (1993).
- ⁵⁷ J. Mateos, T. Gonzalez, and D. Pardo, *J. Appl. Phys.* **77**, 1564 (1995).
- ⁵⁸ J. Mateos, T. Gonzalez, and D. Pardo, *Appl. Phys. Lett.* **67**, 685 (1995).
- ⁵⁹ P. Shiktorov, V. Gruzinskiis, E. Starikov, T. Gonzalez, J. Mateos, D. Pardo, L. Reggiani, and L. Varani, *Appl. Phys. Lett.* **71**, 3093 (1997).
- ⁶⁰ V. Gruzinskiis, E. Starikov, and P. Shiktorov, *Solid-State Electron.* **36**, 1067 (1993).
- ⁶¹ V. Gruzinskiis, E. Starikov, P. Shiktorov, L. Reggiani, M. Saraniti, and L. Varani, *Semicond. Sci. Technol.* **8**, 1283 (1993).
- ⁶² V. Gruzinskiis, E. Starikov, P. Shiktorov, L. Reggiani, and L. Varani, *Appl. Phys. Lett.* **64**, 1662 (1994).
- ⁶³ T. Gonzalez and D. Pardo, *Solid-State Electron.* **39**, 555 (1996).
- ⁶⁴ L. Reggiani, P. Golinelli, E. Faucher, L. Varani, T. Gonzalez, and D. Pardo, in *Proceedings of the 13th International Conference on Noise in Physical Systems and 1/f Fluctuations, Palanga, Lithuania, May 29-June 3, 1995*, edited by V. Bareikis and R. Katilius (World Scientific, Singapore, 1995), p. 163.
- ⁶⁵ V. Gruzinskiis, E. Starikov, and P. Shiktorov, *Phys. Scr.* **T54**, 71 (1994).
- ⁶⁶ E. Starikov, P. Shiktorov, V. Gruzinskiis, L. Reggiani, L. Varani, J. C. Vaissiere, and J. P. Nougier, *Lith. Phys. J.* **35**, 408 (1995).